Real-Time Optimization and Nonlinear Model Predictive Control for a Post-Combustion Carbon Capture Absorber

Gabriel D. Patrón. Luis Ricardez-Sandoval*

**University of Waterloo, Department of Chemical Engineering, Waterloo, ON, N2L 3G1 Canada (Tel: +1 (519)-888-4567 ex:38667; e-mail: laricard@uwaterloo.ca).*

Abstract: A framework to perform real-time optimization (RTO) and nonlinear model predictive control (NMPC) is presented for a post-combustion carbon capture absorber unit. The NMPC is applied as a set point regulator with and without an accompanying RTO scheme. Moreover, a Kalman filter (KF) is used to perform state estimation for the scheme. The absorber RTO formulation considers solvent degradation cost, carbon tax, and electrical pumping costs. The two scenarios (with and without RTO) are assessed in situations with a fixed carbon tax, and a time-varying carbon tax. The results show that the RTO/NMPC scheme provides substantial economic benefit over the NMPC-only scheme, even for a short simulation time (~130 minutes). Furthermore, the RTO also aids in guaranteeing reachable set points for the NMPC, which may not occur otherwise.

Keywords: Real-time Optimization and Control; Nonlinear Process Control; Control of Large-scale Systems

1. INTRODUCTION

As global warming is increasingly in the forefront of public discourse, the drive to develop "green" technologies has never been greater. Chiefly among the causes of global warming is the large quantity of carbon dioxide (CO_2) produced in industrial combustion and emitted in flue gases. To this end, the development of mitigation strategies for CO_2 emissions is essential to restricting further global warming.

Carbon capture and storage (CCS) is one of the technologies on the forefront of CO_2 emission mitigation. This technology aims to sequester CO_2 to avoid its release into the atmosphere, subsequently using it elsewhere or storing it in repositories. There are various ways to achieve CO_2 capture, e.g. pre-combustion, post-combustion, chemical looping combustion, and oxy-combustion. However, post-combustion capture (PCC) holds advantages over the other CCS methods due to its relative maturity. Moreover, PCC can be used to retrofit existing CO_2 emission sources, making its deployment convenient in existing processes. In this work, we focus on a monoethanolamine (MEA)-based chemical absorption PCC method, for which the chemistry and process have been extensively studied (i.e. Dugas, 2006; Hikita et al., 1997). These studies have enabled the development and verification of mathematical models, which in turn, can be used for model-based optimization and control as presented herein.

The control system of the PCC process is crucial in ensuring its productive, safe, and cost-effective operation. As it currently stands, the use of PCC is of net economic detriment to the operation of the upstream power plant with which it is implemented. As such, the economically optimal controlled operation of this process is a crucial aspect that must be investigated in order to encourage widespread adoption of this technology. This can be achieved using what is known as the two-layer approach whereby real-time optimization (RTO) and model predictive control (MPC) are implemented hierarchically, which will be the focus of this study.

While there are many control studies that investigate the dynamic and controlled behaviour of the PCC system (i.e. Åkesson et al., 2012; Sahraei and Ricardez-Sandoval, 2014), the economically optimal operation of this process has not received as much attention. Some notable works in this field include the economically optimal operation of the entire PCC process by Panahi and Skogestad (2012); similarly, single-layer economic model predictive control (EMPC) strategies have been proposed by Decardi-Nelson, Liu and Liu (2018), and Chan and Chen (2018). The literature, however, has not yet considered the implementation of a unit-based two-layer approach; whereby the major PCC units are operated with their own RTO and controller. A decentralized approach such as this allows for increased RTO execution frequency as the economic optimization can be performed upon a single unit reaching steady state (instead of the entire system).

The present study proposes a novel RTO formulation in order to employ the two-layer approach for the PCC absorber. The RTO is accompanied by a nonlinear MPC (NMPC), both of which use a mechanistic model of the PCC absorber. To the authors' knowledge, this is the first work that makes use of an RTO/NMPC formulation for the PCC absorber. In addition to the RTO/NMPC scheme, a Kalman filter (KF) is used to provide state estimates to the layers, another novelty for the PCC absorber. Moreover, this study also investigates the effects of time-varying carbon tax on the RTO/NMPC under transient changes in the operation of the CO_2 capture absorber unit, which has also not been considered previously. Such carbon taxes are becoming increasingly prevalent as CO_2 emission deterrents and their prices may fluctuate subject to market conditions.

This paper is structured as follows: Section 2 introduces the mechanistic PCC absorber model; Section 3 outlines the RTO,

NMPC, and KF formulations proposed in this work; Section 4 presents the results of the proposed formulation implemented in a PCC absorber unit. Concluding remarks and future work are provided in Section 5.

2. PCC ABSORBER MODEL

The dynamic mechanistic absorber model used for the RTO and NMPC scheme in this study was adapted from Harun et al. (2012) and is a partial differential algebraic system of equations (PDAEs). Four chemical species $i = \{MEA, CO_2, H_2O, N_2\}$ are present in the absorber; CO_2 and H_2O exist in both liquid and gas phases, while MEA and N_2 only exist in as liquid and gas, respectively.

During typical operation, the absorption column receives two inlet streams, as depicted in Fig. 1. In a pilot-scale unit, these streams are at opposite sides of the axial domain $z(m)$ with $z = 0\ m$ for the gas inlet, and $z = 6.1\ m$ for the liquid inlet. The flue gas inlet stream contains CO_2, H_2O, and N_2 and comes from an upstream combustion source, while the lean amine solvent stream comes from a holding tank that mixes fresh and recycled solvent and contains MEA, CO_2, and, H_2O. Inside the column, only a small amount of CO_2 is naturally dissolved by the solvent. However, a reactive absorption mechanism uses the weak acid and base properties of CO_2 and MEA, respectively, to create a water-soluble salt that readily dissolves into the lean solvent. This reactive property, in addition to abundance and low cost, makes amine solvents particularly suitable for PCC.

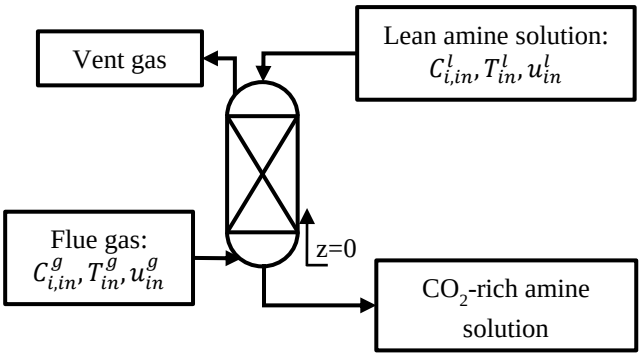

Fig. 1. Absorber column with required inlet conditions.

The model consists of material balances, energy balances, rate equations, chemical kinetic equations, equilibrium equations, and physical property models. These are solved at steady state and dynamically for the RTO and NMPC, respectively. For brevity, the description of the model presented in this work will be limited to the mass and energy balances (differential model), which describe the dynamics of the model states. The phenomenological descriptions (algebraic model) will be omitted for brevity, a full description of the model including the algebraic model can be found elsewhere (Harun et al., 2012). The pilot-scale packed column absorber design characteristics and modelling details can be found in Patron and Ricardez-Sandoval (2020). The model implemented with these design characteristics and inputs produced accurate results with respect to other implementations of the model such as Cerrillo-Briones and Ricardez-Sandoval (2018), and Harun et al. (2012); the latter of which was validated against pilot plant data from Dugas (2006).

2.1 Molar Component Material Balance

The molar component material balances describe the variation in liquid and gas phase component concentrations with respect to position along the column and with respect to time. Variations occur because of changing operating conditions, which lead to changes in mass transfer, reaction rate, and equilibria. They are expressed as follows:

$$\frac{dC_i^l}{dt} = u_l \frac{\partial C_i^l}{\partial z} + a_w N_i \tag{1}$$

$$\frac{dC_i^g}{dt} = -u_g \frac{\partial C_i^g}{\partial z} - a_w N_i - C_i^g \frac{\partial u_g}{\partial z} \tag{2}$$

where $C_i^l(mol/m^3)$ and $C_i^g(mol/m^3)$ are the liquid and gas component concentrations, respectively; $u_l(m/s)$ and $u_g(m/s)$ are the liquid and gas velocities, respectively. $a_w(m^2/m^3)$ is the wetted area inside the absorber and $N_i(mol/m^2/s)$ is the molar component flux between phases. The convention for direction of mass transfer is defined as positive for mass gains to the liquid phase and, consequently, negative for mass gains in the gas phase. While liquid velocity along the height of the column is assumed to be constant, the gas velocity is described as varying due to its substantially lesser density. This is expressed as follows:

$$\frac{\partial u_g}{\partial z} = \frac{u_g}{P}\frac{dP}{dz} + \frac{u_g}{T_g}\frac{dT_g}{dz} - \frac{a_w}{C_{tot}^g}\sum_{i=1}^{4} N_i \tag{3}$$

where $P(bar)$ is the absorber pressure along the axial domain, $T_g(K)$ is the bulk gas phase temperature along the axial domain, and $C_{tot}^g = \sum_{i=1}^{4} C_i^g\ (mol/m^3)$ is the total gas concentration.

2.2 Energy Balance

The energy balances describe the variation in liquid and gas phase bulk temperatures with respect to position along the column and with respect to time. As with the material balances, this variation occurs because of changing operating conditions, which lead to changes in mass transfer, reaction rate, and equilibria. They are expressed as follows:

$$\frac{dT_l}{dt} = u_l \frac{\partial T_l}{\partial z} - \frac{a_w Q_l}{\sum_{i=1}^{4} c_{p,i}^l C_i^l} \tag{4}$$

$$\frac{dT_g}{dt} = -u_g \frac{\partial T_g}{\partial z} + \frac{a_w Q_g}{\sum_{i=1}^{4} c_{p,i}^g C_i^g} \tag{5}$$

where $T_l(K)$ is the bulk gas phase temperature along the axial domain. $Q_l(J/m^3/s)$ and $Q_g(J/m^3/s)$ are the interfacial heat transferred in the liquid and gas phases, respectively; likewise, $c_{p,i}^l(J/mol/K)$ and $c_{p,i}^g(J/mol/K)$ are the molar liquid and gas specific heat capacities, respectively.

3. RTO AND NMPC FORMULATIONS

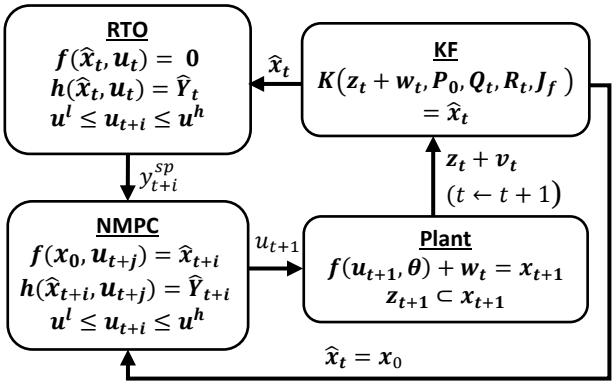

Fig. 2. Arrangement of exchange of information between the RTO, NMPC, KF, and the plant

In this work, the two-layer approach was used to maintain the PCC absorber unit near its economic optimum. Moreover, a KF is used to provide state estimates from measurement. The RTO and NMPC are both formulated as nonlinear optimization problems (NLPs). These are employed in conjunction to affect the plant as depicted in Fig. 2.

3.1 RTO Formulation

The aim of the RTO in the operation of a process is to minimize the operating cost by computing an economically optimal set point at steady state. The RTO designed for the absorber model is formulated as follows:

$$\begin{aligned} &\min_{y_t^{sp}} \mathrm{P_{MEA}} \dot{m}^{l}_{\mathrm{CO_2},out} + \mathrm{P_{CO_2}} \dot{m}^{g}_{\mathrm{CO_2},out} + \mathrm{P_e W_{pump}} \\ &s.t. \\ &\boldsymbol{f}(\boldsymbol{x_t}, \boldsymbol{u_t}) = \boldsymbol{0} \\ &\boldsymbol{h}(\boldsymbol{x_t}, \boldsymbol{u_t}) = \boldsymbol{\hat{Y}_t} \\ &\boldsymbol{u^l} \le \boldsymbol{u_t} \le \boldsymbol{u^h} \end{aligned} \tag{6}$$

where $\dot{m}^{l}_{CO_2,out}(tn/s)$ and $\dot{m}^{g}_{CO_2,out}(tn/s)$ are the liquid and gas outlet CO_2 mass flowrates, respectively. $\mathrm{W_{pump}}$ (kWh/s) is the pump power needed to drive the inlets into the absorber. $y_t^{sp} \in \mathbb{R}^{\mathrm{N_y}}$ is the optimization variable that is passed down as the set point to the NMPC framework, as depicted in Fig. 2. In the case of the PCC absorber column, the optimization variable is the CO_2 removal percentage, defined as follows:

$$\%CC = \frac{F_{in}^{CO_2} - F_{out}^{CO_2}}{F_{in}^{CO_2}} \times 100\% \tag{7}$$

In this study, the economic objective was formulated as the sum of three terms as shown in (6). These correspond to MEA degradation cost (P_{MEA}), the carbon tax cost (P_{CO_2}), and the cost of electricity (P_e). The specific rates for these economic terms are $P_{MEA} = 2.99\ \$CAD\ /tn\ CO_2\ captured$ (adjusted for inflation and converted to $CAD from Singh et al., 2003); $P_{CO_2} = 50\ \$CAD/tn\ CO_2\ emitted$ (Canada.ca, 2019); and $P_e = 0.066\ \$CAD/kWh$ (Auc.ab.ca, 2019), respectively. The MEA degradation cost is incurred owing to the addition of fresh MEA to make up for solvent losses in the process. The carbon tax cost is imposed by state regulatory bodies for releasing CO_2 into the atmosphere. The aforementioned carbon tax rate serves as a nominal value; however, the effect of price variations of this tax will be studied. Lastly, the electricity cost comes from pumping the solvent from an upstream holding tank to the absorber.

$\boldsymbol{f}: \mathbb{R}^{N_x} \times \mathbb{R}^{N_u} \times \mathbb{R}^{N_\theta} \to \mathbb{R}^{N_x}$ represents the set of mass and energy balances stated in (1), (2), (4), and (5), while $\boldsymbol{h}: \mathbb{R}^{N_x} \times \mathbb{R}^{N_u} \times \mathbb{R}^{N_\theta} \to \mathbb{R}^{N_Y}$ are the set of algebraic equations considered in this study, which are not shown here for brevity. These are solved as a steady-state optimization problem for the RTO. $\boldsymbol{\hat{x}_t} \in \mathbb{R}^{N_x}$ and $\boldsymbol{u_t} \in \mathbb{R}^{N_u}$ in (6) are the estimated state and manipulated variable vectors, respectively. These estimated states are provided to the RTO by the KF based on a process model and process measurements. In the case of the absorber model, the states are phase component concentration and temperatures as stated in Section 2. The manipulated variable for the absorber is the solvent flowrate into the column (F_{in}^{l}). $\boldsymbol{u^l}$ and $\boldsymbol{u^h} \in \mathbb{R}^{N_u}$ are the lower ($10\ mol/s$) and upper ($80\ mol/s$) bounds of the manipulated variable, respectively. These bounds are the same as those used in the NMPC framework and reflect the physical limitations of the controller. While these are not necessary to execute the RTO, they are included in the formulation to ensure that the set points determined by the RTO are reachable by the controller. This ensures that the economically optimal set points are feasible by the overall two-layer scheme.

The steady state model was discretized into ten finite elements in the axial domain using finite differences. Model validation showed that the implementation of the absorber model was in good agreement with previous implementations of the model. For the purposes of this study, the RTO is executed at a fixed 100 NMPC sampling intervals (~21 minutes). Preliminary simulations found that this was sufficient time for the NMPC to reach the setpoints dictated by the RTO for the sizes of disturbances in this study; thus, no steady-state detection measure was used. Furthermore, this study assumes that the model parameters do not change substantially during operation, thus no data reconciliation step is implemented. These two issues will be addressed in future work.

3.2 NMPC Formulation

The NMPC aims to drive the system towards the set point indicated by the RTO as depicted in Fig. 2. It does so by solving an optimal control problem at every sampling interval Δt. The NMPC is formulated for the present study as follows:

$$\begin{aligned} &\min_{\boldsymbol{u_{t+j}}\ \forall j \in \{1,\dots,C\}} \boldsymbol{Q} \sum_{i=1}^{P} \left(\boldsymbol{\hat{y}_{t+i}} - \boldsymbol{y^{sp}_{t+i}}\right)^2 + \boldsymbol{R} \sum_{j=1}^{C} \Delta \boldsymbol{u_{t+j}}^2 \\ &s.t. \\ &\boldsymbol{f}\left(\boldsymbol{x_t}, \boldsymbol{u_{t+j}}\right) = \boldsymbol{\hat{x}_{t+i}}; \qquad \forall i \in \{1,\dots,P\},\ \forall j \in \{1,\dots,C\} \\ &\boldsymbol{\hat{x}_t} = \boldsymbol{x_0} \\ &\boldsymbol{h}\left(\boldsymbol{\hat{x}_{t+i}}, \boldsymbol{u_{t+j}}\right) = \boldsymbol{\hat{Y}_{t+i}}; \qquad \forall i \in \{1,\dots,P\},\ \forall j \in \{1,\dots,C\} \\ &\boldsymbol{u^l} \le \boldsymbol{u_{t+j}} \le \boldsymbol{u^h}; \qquad \forall j \in \{1,\dots,C\} \end{aligned} \tag{8}$$

where the objective function is comprised of a set point tracking and a control move suppression term, with the

respective weights $\mathbf{Q} \in \mathbb{R}^{N_y \times N_y}$ and $\mathbf{R} \in \mathbb{R}^{N_u \times N_u}$. $\hat{\boldsymbol{y}}_{t+i} \in \mathbb{R}^{N_y}$ is the controlled variable on the prediction horizon P, whose squared deviation from the setpoint supplied by the RTO ($\mathbf{y}_{t+i}^{sp}$) is minimized. As indicated above, the controlled variable for the absorber NMPC is the %CC, which corresponds to the optimization variable from the RTO. $\Delta \boldsymbol{u}_{t+i} \in \mathbb{R}^{N_u}$ is the vector of change in the manipulated variable ($i.e. \Delta \boldsymbol{u}_{t+i} = \boldsymbol{u}_{t+i} - \boldsymbol{u}_{t+i-1}$) on the control horizon C, the square of which is also minimized subject to the weight $\mathbf{R}$ to prevent rapid changes in the manipulated variable. $\boldsymbol{f}$ in this case represents the time-discretized differential dynamic state model in (1), (2), (4), and (5); while $\boldsymbol{h}$ now represented the time-discretized set of algebraic equations from Harun et al. (2012). As mentioned above, the RTO solves a steady-state optimization problem, thus does not require time discretization; in contrast, the NMPC solves a dynamic optimization problem. $\hat{\boldsymbol{x}}_{t+i} \in \mathbb{R}^{N_x}$ represents the vector of state predictions produced by the dynamic model in the horizon P. This optimization problem is solved in open-loop at every NMPC sampling interval Δt and produces a series of control actions $\boldsymbol{u}_{t+1}, \ldots, \boldsymbol{u}_{t+C}$. The first of the control actions is given to the plant as shown in Fig. 2. The plant is subsequently operated for the sampling interval Δt and the evolved states ($\boldsymbol{x}_0 \in \mathbb{R}^{N_x}$) are passed to the NMPC in a feedback manner as initial conditions, thus closing the loop. These evolved states are estimated using the KF filter based on a process model and measurements.

The NMPCs weighing matrices are set to be identity matrices of proper dimensions (i.e. $\boldsymbol{Q} = \boldsymbol{I}^{\boldsymbol{1}}$ and $\boldsymbol{R} = \boldsymbol{I}^{\boldsymbol{1}}$). The prediction and control horizons are both chosen to be 100 seconds, discretized into eight 12.5 second intervals using three-point Radau collocations. We express the horizons as integer multiples of the intervals (i.e. $P = C = 8$). This discretization was chosen based on preliminary studies, which elucidated that a fine time discretization was necessary due to fast disturbance responses. It was also found that larger sampling intervals posed difficulties for the NLP solver due to model nonlinearities. As with the steady state RTO model, the dynamic NMPC model was discretized into ten finite elements in the axial domain. The coarse axial discretization was chosen in order be parsimonious as a higher resolution discretization in the axial domain would have resulted in a larger number of equations for the solver to consider in the optimization problems. This is especially important for the dynamic NMPC problem, which also must be discretized in time.

3.3 KF Formulation

The axially discretized absorber model has 110 states, which are required to execute the RTO and NMPC. However, it is unlikely that all the states will be available for measurement during the operation of the absorber. Accordingly, a Kalman filter (KF) was used as a state estimator in the proposed scheme. In the current KF scheme, access to all temperatures, gas concentrations, as well as inlet and outlet (boundary) states is assumed, totalling to 74 states. Contrastingly, all interior liquid states, totalling to 36, are estimated. The measured states $\boldsymbol{z}_t \in \mathbb{R}^{N_z}$, where $\boldsymbol{z}_t \subset \boldsymbol{x}_t$, are used to predict all of states $\hat{\mathbf{x}}_t \in \mathbb{R}^{N_x}$. Additionally, randomly sampled process ($\boldsymbol{w}_t \in \mathbb{R}^{N_x}$) and measurement ($\boldsymbol{v}_t \in \mathbb{R}^{N_z}$) noises were introduced to the plant. These noises introduce uncertainty and plant-model mismatch into the system. The nonlinear mechanistic model was used to perform *a priori* state predictions, while the discretized equations were symbolically differentiated to produce the Jacobian matrix $\boldsymbol{J}_f \in \mathbb{R}^{N_x \times N_x}$ for the KF to yield *a posteriori* estimates. The initial state covariance matrix $\mathbf{P_0} \in \mathbb{R}^{N_x \times N_x}$, the process covariance matrix $\mathbf{Q}_t \in \mathbb{R}^{N_x \times N_x}$, and measurement covariance matrix $\mathbf{R}_t \in \mathbb{R}^{N_z \times N_z}$ were defined as follows:

$$\begin{aligned} \mathbf{P_0} &= {\sigma_{P_0}}^2 \mathrm{diag}({x_{1,nom}}^2, \ldots, {x_{N_x,nom}}^2) \\ \mathbf{Q_t} &= {\sigma_{Q_t}}^2 \mathrm{diag}({x_{1,nom}}^2, \ldots, {x_{N_x,nom}}^2) \\ \mathbf{R_t} &= {\sigma_{R_t}}^2 \mathrm{diag}({z_{1,nom}}^2, \ldots, {z_{N_z,nom}}^2) \end{aligned} \quad (9)$$

where $x_{i,nom} \forall i\{1, \ldots, N_x\}$ and $z_{i,nom} \forall i\{1, \ldots, N_z\}$ are the states and measurements during nominal operation, described in the following section. $\sigma_{P_0} = \sigma_{Q_t} = 1e^{-5}$ and $\sigma_{R_t} = 1e^{-6}$ are the corresponding matrix weights. The complete KF scheme is denoted as $\boldsymbol{K}: \mathbb{R}^{N_z} \rightarrow \mathbb{R}^{N_x}$ for brevity in Fig. 2. As with the NMPC, the KF was executed every sampling interval (12.5 s).

4. RESULTS

Three test scenarios were implemented to assess the performance of the RTO/NMPC implementation. The scenarios were subjected to the series of disturbances depicted in Fig. 3. These disturbances impose different sizes and directions of steps every 100 NMPC sampling intervals and were chosen to represent substantial variation around the nominal inlet flue gas flowrate (from 0.8 to 1.2 times its nominal value of 4.012 mol/s), which can be considered as the main disturbance that will affect the operation of this unit. The test scenarios included observing the effects of a fixed and a varying carbon tax; the fixed price tax case used a price of 50\$CAD/tn CO_2 emitted, while the varying carbon tax cost features subsequent 5\$CAD steps up from the base price of 50\$CAD/tn CO_2 emitted as displayed in Fig. 4.

The test scenarios, presented next, correspond to 1) no RTO implemented (only regulation by NMPC to the initial nominal set-point), 2) RTO /NMPC framework (Fig. 2) with a fixed carbon tax, and 3) RTO/NMPC framework with a varying carbon tax (Fig. 4). In all scenarios, the disturbance followed the trajectory shown in Fig. 3 whereby it is at its nominal value for 25 sampling intervals (~5 minutes) and a step change is introduced every 100 sampling intervals (~21 minutes) thereafter. The inlet solvent flowrate (manipulated variable) and percent carbon captured (controlled variable) results for these scenarios are shown in Fig. 5 and Fig. 6, respectively.

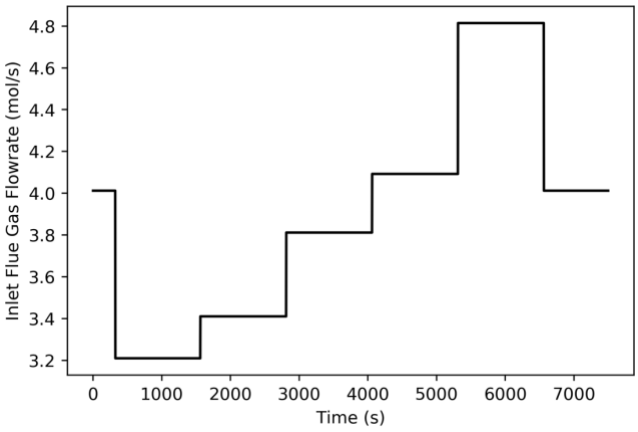

Fig. 3. Inlet flue gas flowrate (disturbance).

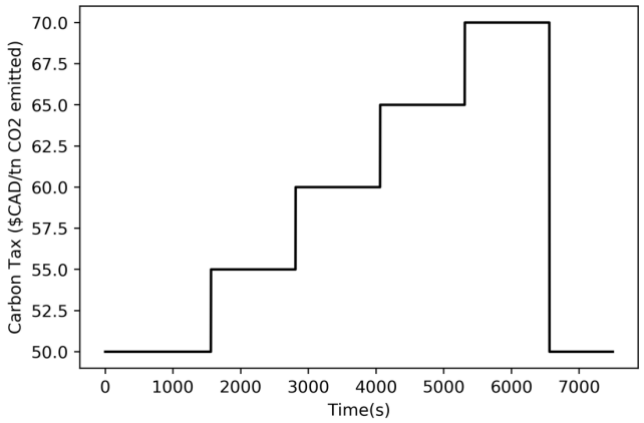

Fig. 4. Carbon tax profile for varying tax case.

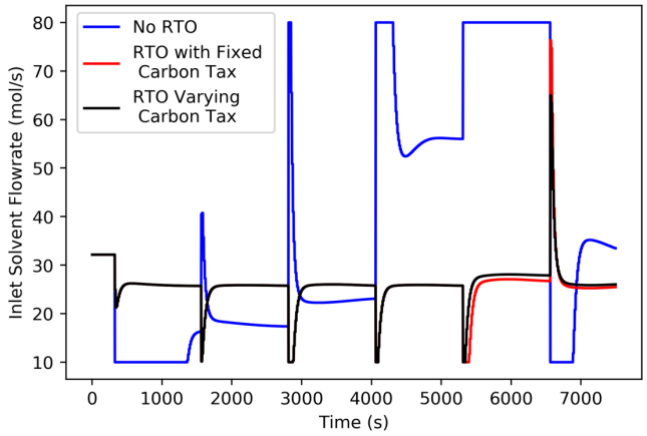

Fig. 5. Inlet solvent flowrate (manipulated variable) for the scenarios tested.

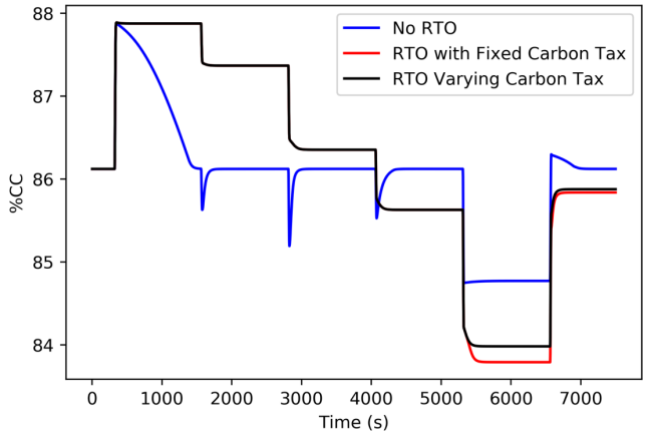

Fig. 6. Percent carbon captured (controlled variable) for the scenarios tested.

The scenarios were assessed on the basis of their process cost from the first to the final disturbance, these results are displayed in Table 1. The costs were calculated using the expression employed in the RTO objective function shown in (6). This instantaneous price rate is multiplied by the time interval lengths to give a total process cost comprised of the MEA degradation, carbon tax, and electricity cost over the operating period considered in this study. The total cost is also broken down into its aforementioned sources. The results for each scenario are discussed next.

Table 1. Process cost for scenarios tested ($CAD).

Scenario	Total Cost	Tax Cost	MEA Cost	Electrical Cost
No RTO (fixed tax)	13.46	6.31	7.13	0.01
No RTO (varying tax)	14.64	7.50	7.13	0.01
RTO (fixed tax)	11.98	6.31	5.67	0.01
RTO (varying tax)	13.23	7.51	5.70	0.01

4.1 NMPC Only (No RTO)

The NMPC was implemented without the RTO to regulate the set point subject to the disturbances shown in Fig. 3. The 86.12 %CC set point in this case corresponds to the steady state operation of the absorber using the nominal inlet flue gas fractions reported in Harun et al. (2012). The objective of this case was to establish a "do-nothing" baseline cost, in which no set point updates based on process economics are considered.

It can be observed in Fig. 6 that the controller is able to successfully regulate to the set point for all except one of the disturbances introduced. This exception occurs in the 5th disturbance interval (from ~5300 seconds to ~6600 seconds), and corresponds to a large +18% step-up in the disturbance variable with respect to its nominal value, as shown in Fig. 3. During this period, Fig. 5 shows that the controller holds the manipulated variable at its upper bound (80 mol/s) and despite this, the set point appears to be unreachable as the %CC reaches an asymptote in Fig. 6. This unreachable set point occurs because it becomes increasingly difficult to achieve the same %CC for flue gas flowrates that are largely increased due to the upper bound of the manipulated variable. For this upper solvent flowrate bound and concentration, the solution has been saturated with CO_2 and has no remaining absorption capacity. Typically, the flue gas flowrate serves as a manipulated variable for smaller disturbances (i.e. ±10%). Larger disturbances in the system would be handled by a downstream reboiler or upstream MEA make-up stream that would enrich the concentration of the MEA solvent fed to the absorber, thereby increasing the CO_2 absorption capacity. It is important to note that the issue of unreachable set points could have been avoided by executing RTOs when each disturbance was introduced. This will be shown in the next section.

Using the results from the no-RTO scenario, the process costs were calculated for the fixed and varying tax rates. As noted in Table 1, the cost of this experiment is about 8.77% higher in the varying cost case than the fixed cost case. This increase comes entirely from carbon tax. The increased cost occurs as the fixed cost case considers only the minimum cost in the varying cost case. This disparity would widen with longer periods of operation where the cost can accrue over time.

4.2 NMPC and RTO

The NMPC tested in the previous section was implemented along with the RTO for fixed and varying carbon taxes. From Fig. 5, it is clear that the NMPC is not required to perform as aggressive of control actions in the RTO/NMPC scheme compared to the no-RTO scheme. This is shown in the manipulated variable, which is at bounds substantially less than in the no-RTO scenario. Furthermore, it can be observed

in Fig. 6 that the controller successfully tracks the new set points supplied by the RTO before the next disturbance enters the system for all intervals. In fact, steady state is generally reached quickly, resulting in short transition times. Generally, the control profiles (Fig. 5) for both the RTO/NMPC cases (fixed and varying carbon tax) look similar in shape; however; it can be observed that the RTO selects slightly different removal set points in Fig. 6 for the 5th and 6th disturbances (from ~5300 s to ~7800 s). The 5th disturbance corresponds to a combination in the highest carbon tax rate (70$CAD) and disturbance (4.814 mol/s) entering the process. The confluence of these factors results in the largest RTO set point disparity between the fixed and variable tax cost cases. The 6th disturbance is another large step down in both the flue gas flowrate (-20%) and carbon tax rate (-40%). Aside from these two periods; however, there is not a marked difference between the set points determined by the fixed and varying tax RTOs. This suggests that the RTO is insensitive to carbon tax and disturbance variable changes unless they are large.

The RTO scenario with varying carbon tax incurred significantly (10.43%) more cost than the fixed carbon tax scenario This is to be expected as the tax is increasing from its nominal value, which was considered in the fixed tax case. Nonetheless, the economic benefit of employing the RTO is evident in Table 1, which shows cost reductions of 11.00% and 9.63% for the fixed and varying carbon tax cases, respectively, with respect to the no-RTO cases. Moreover, as shown in Table 1, the RTO in both tax cases gains most of its economic benefit by decreasing the MEA degradation cost, which is reflected in the similar tax cost incurred in these cases. This reinforces the idea that the RTO chooses to reduce costs via the MEA degradation cost and is insensitive to the carbon tax rate unless it is subjected to large changes. These results show economic differences over the short operational time of ~130 min. This would be even further apparent over a longer operational period of hours or days, which a PCC system would experience in real operation. Moreover, this study considers the operation of a pilot-scale unit, the magnitude of these costs would be much higher in industrial-scale.

5. CONCLUSIONS

An RTO/NMPC implementation for a PCC absorber is presented. The implementation of a nonlinear mechanistic dynamic model used to formulate an RTO and an NMPC in tandem is a novelty for this process. It was found that the RTO provided a significant economic improvement for the absorber. Moreover, it was found that although variations in the carbon tax price presented significant economic detriment to the system, which could be mitigated by the RTO. Future works will investigate parameter estimation and model adaptation for the PCC absorber in order to address plant/model mismatch at the RTO level. Despite the good performance of the KF in this study, increased noise or less access to measurements would likely affect the estimates adversely. As such, the use of more advanced state estimation schemes (i.e. moving horizon estimation) will also be investigated in the future. The single-layer approach will also be considered by merging the two formulations presented here into an EMPC. Furthermore, these formulations will be extended from the absorber to include the full PCC plant.

REFERENCES

Åkesson, J., Laird, C., Lavedan, G., Prölß, K., Tummescheit, H., Velut, S. and Zhu, Y. (2012). Nonlinear Model Predictive Control of a CO2 Post-Combustion Absorption Unit. *Chemical Engineering & Technology*, 35(3), pp.445-454.

Auc.ab.ca. (2019). *Current rates and terms of conditions*. [online] Available at: http://www.auc.ab.ca/Pages/current-rates-electric.aspx [Accessed 10 Oct. 2019.].

Canada.ca. (2019). *Pricing carbon pollution in Canada: how it will work*. [online] Available at: https://www.canada.ca/en/environment-climate-change/news/2017/05/pricing_carbon_pollutionincanadahowitwillwork.html [Accessed 10 Oct. 2019].

Cerrillo-Briones, I. and Ricardez-Sandoval, L. (2019). Robust optimization of a post-combustion CO2 capture absorber column under process uncertainty. *Chemical Engineering Research and Design*, 144, pp.386-396.

Chan, L. and Chen, J. (2018). Improving the energy cost of an absorber-stripper CO2 capture process through economic model predictive control. *International Journal of Greenhouse Gas Control*, 76, pp.158-166.

Decardi-Nelson, B., Liu, S. and Liu, J. (2018). Improving Flexibility and Energy Efficiency of Post-Combustion CO2 Capture Plants Using Economic Model Predictive Control. *Processes*, 6, 135.

Dugas, E. (2006). *Pilot plant study of carbon dioxide capture by aqueous monoethanolamine*. Master's Thesis. The University of Texas at Austin.

Harun, N., Nittaya, T., Douglas, P., Croiset, E. and Ricardez-Sandoval, L. (2012). Dynamic simulation of MEA absorption process for CO2 capture from power plants. *International Journal of Greenhouse Gas Control*, 10, pp.295-309.

Hikita, H., Asai, S., Ishikawa, H. and Honda, M., 1977. The kinetics of reactions of carbon dioxide with monoethanolamine, diethanolamine and triethanolamine by a rapid mixing method. *The Chemical Engineering Journal*, 13(1), pp.7-12.

Panahi, M. and Skogestad, S. (2012). Economically efficient operation of CO2 capturing process. Part II. Design of control layer. *Chemical Engineering and Processing: Process Intensification*, 52, pp.112-124.

Patron, G. and Ricardez-Sandoval, L., 2020. A robust nonlinear model predictive controller for a post-combustion CO2 capture absorber unit. *Fuel*, 265, 116932.

Hossein Sahraei, M. and Ricardez-Sandoval, L. (2014). Controllability and optimal scheduling of a CO 2 capture plant using model predictive control. *International Journal of Greenhouse Gas Control*, 30, pp.58-71.

Singh, D., Croiset, E., Douglas, P. and Douglas, M. (2003). Techno-economic study of CO2 capture from an existing coal-fired power plant: MEA scrubbing vs. O2/CO2 recycle combustion. *Energy Conversion and Management*, 44(19), pp.3073-3091.